



Cite this: *New J. Chem.*, 2019, 43, 18003

# Hydrogenation of levulinic acid to valeric acid over platinum–tungsten catalysts supported on $\gamma$ -Al<sub>2</sub>O<sub>3</sub>

Ponnala Bhanuchander,<sup>a</sup> Shanthi Priya Samudrala,<sup>ib</sup>\*<sup>b</sup> Balla Putrakumar,<sup>c</sup> Perupogu Vijayanand,<sup>d</sup> Beepala Sateesh Kumar<sup>a</sup> and Komandur V. R. Chary\*<sup>a</sup>

To address the challenges associated with fossil fuel depletion, exploration of the sustainable energy resources is one of the most pursued research areas in this century. Valeric acid (VA) is considered as a valuable platform molecule for the production of biofuels and chemical intermediates. However, the production of VA from levulinic acid (LA) has become one of the most desirable reactions. The aim of this work was to investigate the amount of acidity, Pt loading and experimental conditions for the hydrogenation of LA into VA operated at 0.1 MPa H<sub>2</sub> pressure and to elucidate the relationship between the active sites and the catalytic performance. The Pt–WO<sub>3</sub> catalysts supported on  $\gamma$ -Al<sub>2</sub>O<sub>3</sub> were synthesized by a simple wet impregnation method with various Pt loadings from 0.5 to 3 wt% with constant 10 wt% of WO<sub>3</sub> and calcination at 500 °C for 4 h under air. The catalysts were characterized by powder X-ray diffraction (XRD), scanning electron microscopy-energy dispersive X-ray spectroscopy (SEM-EDS), N<sub>2</sub> adsorption–desorption, temperature programmed desorption of ammonia (NH<sub>3</sub>-TPD), pyridine Fourier transform infrared spectroscopy (Pyr.FT-IR) and CO-chemisorption studies. Under optimized reaction conditions, the 2Pt–10WO<sub>3</sub>/ $\gamma$ -Al<sub>2</sub>O<sub>3</sub> catalyst exhibited the highest selectivity to VA (58%) with 91% conversion of LA. This is due to the availability of a huge number of acidic and Pt active sites on the catalyst surface. In addition, the catalytic activity, reaction parameters and stability of the catalyst are demonstrated clearly.

Received 5th August 2019,  
Accepted 21st October 2019

DOI: 10.1039/c9nj04056k

rsc.li/njc

## 1. Introduction

To address the challenges associated with fossil fuel depletion, exploration of sustainable energy resources is one of the most pursued research areas in this century.<sup>1–6</sup> Biomass technology has become unique among the various available sustainable energy strategies such as solar, wind, geothermal, *etc.* Levulinic acid (LA) is recognized by the U.S. Department of Energy as one of the most valuable chemicals from lignocellulose and its derivatives are important biomass building block molecules to obtain products ranging from cosmetics to fuel additives.<sup>7–11</sup>

Valeric acid (VA) is considered as a valuable platform molecule to produce biofuels and chemical intermediates.<sup>12–16</sup> Moreover, VA is considered as a potential solvent for biomass conversion.

Therefore, the synthesis of valeric acid from levulinic acid has become one of the most desirable reactions during the past decade.

In a pioneering research study,<sup>17</sup> solid base catalysts were found to be the most active for the hydrogenation of LA to GVL. Nevertheless, limited reports exist for the direct conversion of LA to VA. Lange *et al.*<sup>18</sup> studied the multi-step synthesis of valeric acid from LA using a Pt/TiO<sub>2</sub> catalyst. Weckhuysen *et al.*<sup>16</sup> explored the Ru catalyst on supported zeolite for the conversion of levulinic acid to valeric acid and obtained 45.8% yield by employing dioxane as solvent at 200 °C and 40 bar H<sub>2</sub> pressure. Kon *et al.*<sup>19</sup> explored the catalytic hydrogenation of LA to VA over a Pt/HMFL catalyst at 200 °C and 8 bar H<sub>2</sub> pressure. Fu *et al.*<sup>20</sup> reported levulinic acid hydrogenation on a Ru/SBA–SO<sub>3</sub>H catalyst in ethanol that resulted in the co-production of valeric acid and ethyl valerate with 94% yield at 240 °C and 40 bar H<sub>2</sub> pressure. Although the catalytic systems demonstrate direct VA synthesis, the present procedures are neither competent nor cost-effective.

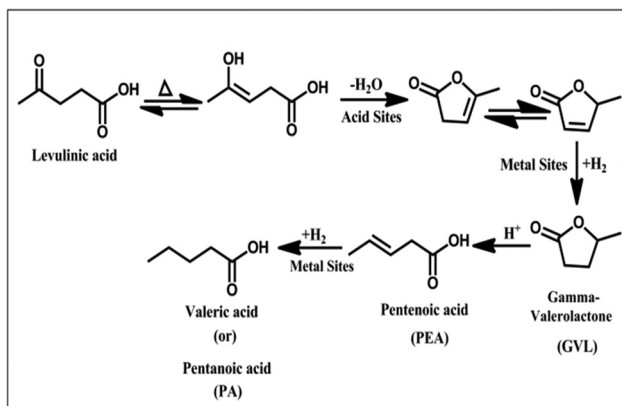
Noble metal-based catalysts have attracted significant consideration due to their wide applications as catalysts in reactions such as hydrogenation, dehydrogenation and oxidation. The supported noble metal catalysts (*e.g.*, Ru, Rh, Pd, Pt and Au) are the most

<sup>a</sup> Catalysis and Fine Chemicals Division, CSIR-Indian Institute of Chemical Technology, Uppal Road, Hyderabad 500007, India. E-mail: kvrchary@iict.res.in, charykvr@gmail.com

<sup>b</sup> Department of Chemical Engineering, Monash University, Melbourne, 3800, Australia. E-mail: priya.shanthipriya@monash.edu

<sup>c</sup> State Key Laboratory of Catalysis, Dalian Institute of Chemical Physics, Chinese Academy of Sciences, Dalian, China

<sup>d</sup> Centre for Environmental Engineering & Fossil Fuels Division, CSIR-Indian Institute of Chemical Technology, Uppal Road, Hyderabad 500007, India



Scheme 1 Selective hydrogenation of LA to VA over Pt-WO<sub>3</sub>/γ-Al<sub>2</sub>O<sub>3</sub>.

commonly used catalysts to produce GVL from LA in the continuous and batch reactors. Several results indicate that noble metal-based catalysts have shown higher activity for hydrogenation of LA to GVL in both homogeneous and heterogeneous systems. But, the enormously high cost and rare resources limit their large-scale applications. Hence, it is necessary to expand the exploitation of noble metals. Various efforts have been devoted to improving the catalytic efficiency by dispersing noble metal catalysts onto an appropriate support with high surface area, such as metallic oxides. Among the various support materials, Al<sub>2</sub>O<sub>3</sub> based materials have received significant research interest due to their decent electronic properties, good surface area and excellent thermal stability.

The aim of this work was to investigate the impact of acidity, Pt loading and experimental conditions on LA conversion into VA over 2Pt-10WO<sub>3</sub>/γ-Al<sub>2</sub>O<sub>3</sub> at 0.1 MPa H<sub>2</sub> pressure and to elucidate the relationship between the active sites and catalytic performance. Characterization techniques including N<sub>2</sub> adsorption-desorption isotherms, temperature-programmed desorption of NH<sub>3</sub> (NH<sub>3</sub>-TPD), powder X-ray diffraction (XRD), UV-diffuse reflectance spectra, scanning electron microscopy-energy dispersive X-ray spectroscopy (SEM-EDS), CHNS analysis and transmission electron microscopy were employed to comprehend the development of the catalyst structure and the physicochemical properties. New insights into the parameters that govern the catalytic activity, selectivity and stability are highlighted (Scheme 1).

## 2. Results and discussion

### 2.1 Catalyst characterization

**2.1.1 X-ray diffraction (XRD) analysis.** Fig. 1 presents the XRD patterns of Pt-10WO<sub>3</sub>/Al<sub>2</sub>O<sub>3</sub> catalysts with various Pt loadings (0.5 to 3 wt%). The XRD pattern of 10WO<sub>3</sub>/Al<sub>2</sub>O<sub>3</sub> exhibited three broad diffraction peaks at 39.5°, 45.8° and 66.7°, which correspond to the (222), (400) and (440) cubic crystalline phase of Al<sub>2</sub>O<sub>3</sub> (ref. pattern. 00-001-1303), and did not show any diffraction peaks due to WO<sub>3</sub>, indicating that tungsten species mainly existed in the amorphous structure on the γ-Al<sub>2</sub>O<sub>3</sub> support. After Pt loading, XRD patterns showed three sharp diffraction peaks at around 39.7°, 46.3° and 67.3°, which can be attributed to the (111), (200) and

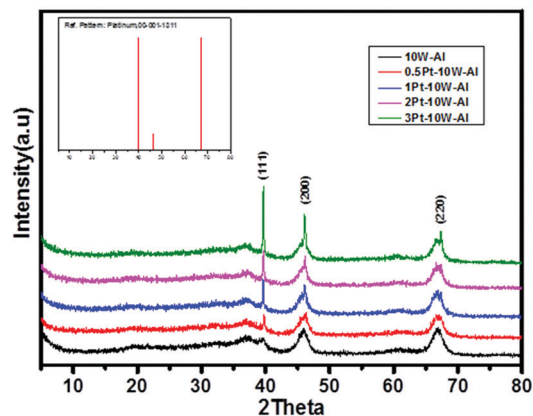


Fig. 1 XRD patterns of 10WO<sub>3</sub>/γ-Al<sub>2</sub>O<sub>3</sub> and various Pt-10WO<sub>3</sub>/γ-Al<sub>2</sub>O<sub>3</sub> catalysts.

(220) lattice planes of Pt (ref. pattern. 00-001-1311).<sup>21</sup> These peaks are gradually sharpened from sample 0.5Pt-10WO<sub>3</sub>/Al to 3Pt-10WO<sub>3</sub>/Al, revealing that an increase in the Pt amount increased the Pt particle size.

**2.1.2 CO-chemisorptions.** The platinum dispersion, metal surface area and average particle size of XPt-10WO<sub>3</sub>/γ-Al<sub>2</sub>O<sub>3</sub> catalysts with different platinum loadings (0.5–3 wt%) were measured using irreversible CO-chemisorption and the results are presented in Table 1. These results demonstrated that up to 2 wt% of platinum content, the CO uptake value was increased (from 4.25 to 5.79) and with a further increase of Pt content beyond 2 wt%, the CO-uptake value was decreased (3.25). The metal surface area of the 10WO<sub>3</sub>/γ-Al<sub>2</sub>O<sub>3</sub> catalyst with different platinum loadings was found to be in the range of 0.28–0.40 m<sup>2</sup> g<sup>-1</sup> whereas the particle size varied between 8.20 and 22.95 nm. With the increase of platinum loading from 0.5 to 3 wt% on the WO<sub>3</sub>/γ-Al<sub>2</sub>O<sub>3</sub> catalyst a decrease in platinum dispersion was observed. These effects are probably due to the agglomeration of platinum particles over the support. The introduction of tungstate particles into the catalyst led to a decrease in the dispersion of Pt.

**2.1.3 BET surface area and pore size distribution studies.** The BET surface area, pore volume and average pore diameter of pure γ-Al<sub>2</sub>O<sub>3</sub>, 10WO<sub>3</sub>/γ-Al<sub>2</sub>O<sub>3</sub> and XPt-10WO<sub>3</sub>/γ-Al<sub>2</sub>O<sub>3</sub> catalysts with different platinum loadings are presented in Table 2. The pure γ-Al<sub>2</sub>O<sub>3</sub> and 10WO<sub>3</sub>/γ-Al<sub>2</sub>O<sub>3</sub> samples had a BET surface area of 235 m<sup>2</sup> g<sup>-1</sup> and 205 m<sup>2</sup> g<sup>-1</sup> respectively. After impregnation of WO<sub>3</sub> and Pt on the support, the BET surface area of Pt with

Table 1 Results of dispersion, CO uptake, metal area, and average particle size of 2Pt-10WO<sub>3</sub>/γ-Al<sub>2</sub>O<sub>3</sub> catalysts

Catalyst	(a)	(b)	(c)	(d)
0.5Pt-10WO <sub>3</sub> /γ-Al <sub>2</sub> O <sub>3</sub>	11.37	4.25	0.32	8.20
1Pt-10WO <sub>3</sub> /γ-Al <sub>2</sub> O <sub>3</sub>	10.07	5.60	0.38	14.25
2Pt-10WO <sub>3</sub> /γ-Al <sub>2</sub> O <sub>3</sub>	8.22	5.79	0.40	18.29
3Pt-10WO <sub>3</sub> /γ-Al <sub>2</sub> O <sub>3</sub>	6.74	3.25	0.28	22.95

a – dispersion (%), b – CO uptake (μmol g<sup>-1</sup>), c – metal surface area (m<sup>2</sup> g<sup>-1</sup>)<sub>cat</sub>, d – particle size (nm).

**Table 2** Physicochemical properties  $\gamma$ -Al<sub>2</sub>O<sub>3</sub> and  $\gamma$ -Al<sub>2</sub>O<sub>3</sub> supported catalysts

Catalyst	(a)	(b)	(c)
Pure $\gamma$ -Al <sub>2</sub> O <sub>3</sub>	235	6.2	0.45
10WO <sub>3</sub> / $\gamma$ -Al <sub>2</sub> O <sub>3</sub>	205	5.2	0.32
0.5Pt-10WO <sub>3</sub> / $\gamma$ -Al <sub>2</sub> O <sub>3</sub>	195	4.6	0.23
1Pt-10WO <sub>3</sub> / $\gamma$ -Al <sub>2</sub> O <sub>3</sub>	172	4.3	0.18
2Pt-10WO <sub>3</sub> / $\gamma$ -Al <sub>2</sub> O <sub>3</sub>	167	4.0	0.16
3Pt-10WO <sub>3</sub> / $\gamma$ -Al <sub>2</sub> O <sub>3</sub>	153	3.8	0.12

a – BET surface area (m<sup>2</sup> g<sup>-1</sup>), b – pore diameter (nm), c – pore volume (cc g<sup>-1</sup>).

various loadings (0.5 to 3 wt%) decreased from 195 to 153 m<sup>2</sup> g<sup>-1</sup> as compared to pure  $\gamma$ -Al<sub>2</sub>O<sub>3</sub> which could be due to the blocking of  $\gamma$ -Al<sub>2</sub>O<sub>3</sub> pores by the deposition of Pt and tungstate species. The results are shown in Fig. 2, and it was observed that the pore volume and pore diameter of  $\gamma$ -Al<sub>2</sub>O<sub>3</sub> supported catalysts decreased from 0.32 to 0.12 cc g<sup>-1</sup> and from 5.2 to 3.8 nm respectively. These results are in accordance with the previous reports.<sup>22</sup>

N<sub>2</sub> adsorption–desorption measurement results are presented in Fig. 2. The isotherm of 10WO<sub>3</sub>/ $\gamma$ -Al<sub>2</sub>O<sub>3</sub> shows a sharp uptake at low relative pressure ( $P/P_0 < 0.015$ ) but a hysteresis loop at high relative pressure ( $P/P_0 > 0.45$ ), which confirms the existence of abundant micropore and meso/macropore structures in the materials. The Brunauer–Emmett–Teller (BET) surface area of 10WO<sub>3</sub>/ $\gamma$ -Al<sub>2</sub>O<sub>3</sub> was found to be 190.7 m<sup>2</sup> g<sup>-1</sup> with a pore volume of 0.238 cc g<sup>-1</sup> and an average pore diameter of 53.2 Å.

**2.1.4 SEM-EDX.** The elemental mapping (Al, O, W and Pt elements) and the energy dispersive X-ray spectroscopy (EDX) analysis of the 2Pt-10WO<sub>3</sub>/ $\gamma$ -Al<sub>2</sub>O<sub>3</sub> catalyst have been conducted to further explore the composition and elemental distribution of the catalysts. EDX elemental mapping images indicate the existence of Al, W, O and Pt elements on the surfaces of the 2Pt-10WO<sub>3</sub>/ $\gamma$ -Al<sub>2</sub>O<sub>3</sub> catalyst. Al and O elements are extremely homogeneously distributed along with the catalyst, as observed

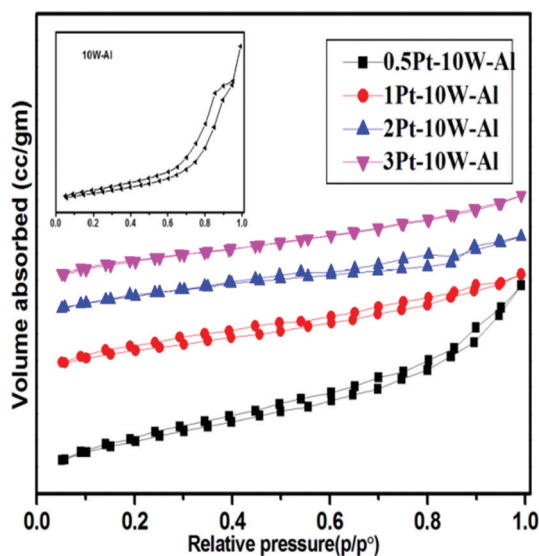


**Fig. 2** BET isotherms of 10WO<sub>3</sub>/ $\gamma$ -Al<sub>2</sub>O<sub>3</sub> (inset figure) and various 10WO<sub>3</sub>/ $\gamma$ -Al<sub>2</sub>O<sub>3</sub> supported platinum catalysts.

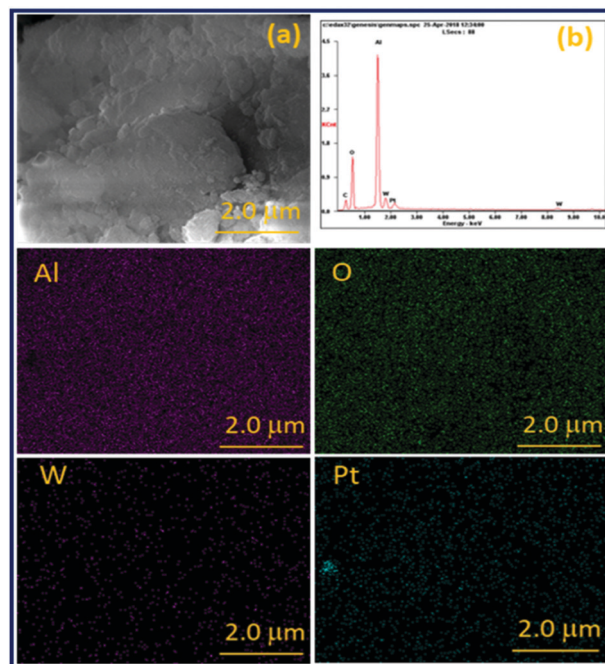


**Fig. 3** (a) SEM and (b) EDX results and the corresponding elemental mapping images of 2Pt-10WO<sub>3</sub>/ $\gamma$ -Al<sub>2</sub>O<sub>3</sub> catalysts.

in Fig. 3. W and Pt mapping images reveal separated and well distributed W and Pt particles over the support. These results demonstrate that W and Pt have been successfully and uniformly incorporated into the alumina framework.

**2.1.5 Transmission electron microscopy.** The morphology of the as-synthesized materials was investigated by transmission electron microscopy (TEM). The TEM image of 10WO<sub>3</sub>/ $\gamma$ -Al<sub>2</sub>O<sub>3</sub> reveals that the composite material has a rod-like structure with different sizes. After impregnation of platinum the rod became smaller and wider. The results are shown in Fig. 4.

**2.1.6 UV-visible diffusion reflectance spectra.** The UV-vis diffused reflectance spectra of the various Pt-10WO<sub>3</sub>/ $\gamma$ -Al<sub>2</sub>O<sub>3</sub> catalysts were recorded in the range of 200 to 600 nm and the results are shown in Fig. 5. The UV-vis diffused reflectance spectra of the 2Pt-10WO<sub>3</sub>/ $\gamma$ -Al<sub>2</sub>O<sub>3</sub> sample show one intensive absorption band at 211.6 nm and two weak and broad absorption bands at 270.3 and 374.4 nm. The main absorption band corresponds to the ligand to metal charge transfer in isolated

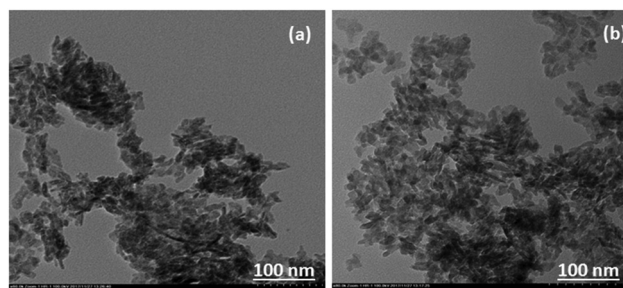


**Fig. 4** TEM images of (a) 10WO<sub>3</sub>/ $\gamma$ -Al<sub>2</sub>O<sub>3</sub> and (b) 2Pt-10WO<sub>3</sub>/ $\gamma$ -Al<sub>2</sub>O<sub>3</sub> catalysts.

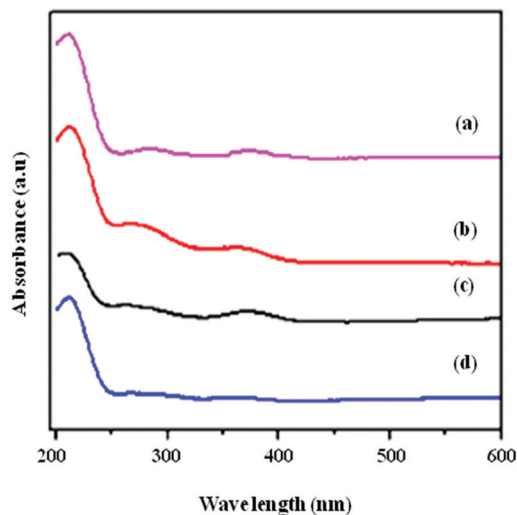


Fig. 5 UV-DRS patterns of the various  $10\text{WO}_3/\gamma\text{-Al}_2\text{O}_3$  supported platinum catalysts. (a)  $0.5\text{Pt}-10\text{WO}_3/\gamma\text{-Al}_2\text{O}_3$ , (b)  $1\text{Pt}-10\text{WO}_3/\gamma\text{-Al}_2\text{O}_3$ , (c)  $2\text{Pt}-10\text{WO}_3/\gamma\text{-Al}_2\text{O}_3$  and (d)  $3\text{Pt}-10\text{WO}_3/\gamma\text{-Al}_2\text{O}_3$ .

tetrahedral species. The weak charge transfer bands around 270 nm and 375 nm are due to the charge transfer of  $\text{O}^{2-}$  to  $\text{W}^{6+}$  in an octahedrally coordinated tungsten oxide species and the presence of bulk  $\text{WO}_3$  crystallites respectively.<sup>23</sup> With the increase in Pt loading, the intensity of these charge transfer bands gradually weakened and slightly shifted to a higher wavelength range.

**2.1.7 Temperature programmed reduction.** The temperature programmed reduction (TPR) pattern of  $X\text{Pt}-10\text{WO}_3/\gamma\text{-Al}_2\text{O}_3$  catalysts with various platinum loadings (0.5 to 3 wt%) is shown in Fig. 6 and the  $\text{H}_2$  uptake values are displayed in Table 3. All the catalysts have shown the  $\text{H}_2$ -TPR profile within the temperature range of 50–800 °C. The bulk  $\text{WO}_3$  showed three main peaks in the  $\text{H}_2$ -TPR profile with maxima at 630, 790, and 910 °C in accordance with the previous reports.<sup>24,25</sup>

The TPR analysis of various  $\text{Pt}-10\text{WO}_3/\gamma\text{-Al}_2\text{O}_3$  samples exhibited reduction peaks at 640 °C and 790 °C which indicate the presence of  $\text{WO}_3$  species on the  $\gamma\text{-Al}_2\text{O}_3$  support.<sup>26,27</sup> The reduction peak at 640 °C is associated with the partial reduction of  $\text{WO}_3$  to tungsten-oxide ( $\text{WO}_{2.9}$ ), whereas the simultaneous reduction of  $\text{WO}_{2.9}$  oxide and of the remaining  $\text{WO}_3$  to  $\text{WO}_2$  phase occurs at approximately 790 °C. Another reduction peak at 355 °C indicates reduction of Pt to the metallic phase ( $\text{Pt}^{2+}$  to  $\text{Pt}^0$ ) for the  $\text{Pt}-\text{WO}_3$  catalyst supported on  $\gamma\text{-Al}_2\text{O}_3$ .<sup>28</sup> Therefore, the reduction peaks observed must be due to the reduction of Pt and  $\text{WO}_3$  only and the results are presented in Fig. 6.

**2.1.8 Temperature programmed desorption of ammonia.** The TPD of ammonia is used to determine the strength of acidic sites on a catalyst surface. The total acidity of the catalyst and the results obtained are presented in Table 4. In general, the  $\text{NH}_3$ -TPD peaks are classified into three different acid sites based on their strength: weak acid sites at 150–300 °C, medium acid sites at 300–400 °C and strong acid sites at 450–650 °C.<sup>29</sup> Fig. 7 presents  $\text{NH}_3$ -TPD profiles showing the presence of only two types of peaks, which are at low and high temperatures, over the catalyst surface. The  $\text{NH}_3$ -TPD curve of the  $\text{Pt}-\text{WO}_3/\gamma\text{-Al}_2\text{O}_3$

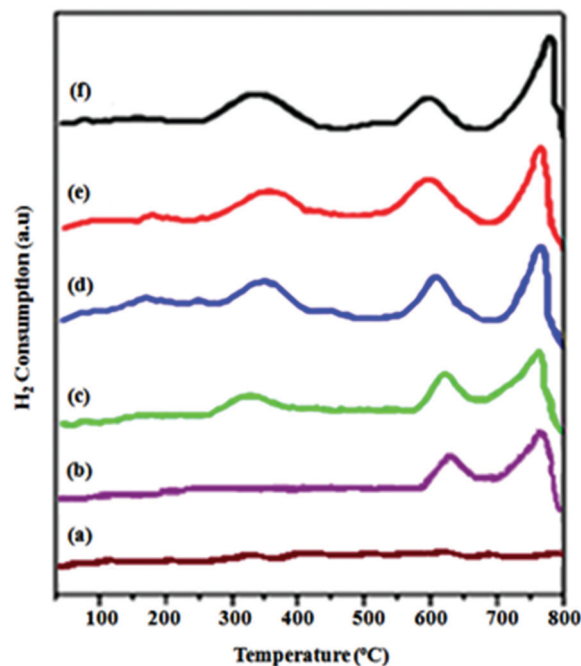


Fig. 6  $\text{H}_2$  TPR profiles of various  $2\text{Pt}-\text{WO}_3/\gamma\text{-Al}_2\text{O}_3$  catalysts. (a)  $\gamma\text{-Al}_2\text{O}_3$ , (b)  $10\text{WO}_3/\gamma\text{-Al}_2\text{O}_3$ , (c)  $0.5\text{Pt}-10\text{WO}_3/\gamma\text{-Al}_2\text{O}_3$ , (d)  $1\text{Pt}-10\text{WO}_3/\gamma\text{-Al}_2\text{O}_3$ , (e)  $2\text{Pt}-10\text{WO}_3/\gamma\text{-Al}_2\text{O}_3$  and (f)  $3\text{Pt}-10\text{WO}_3/\gamma\text{-Al}_2\text{O}_3$ .

Table 3 Results of temperature programmed reduction of various  $\text{Pt}-\text{WO}_3/\gamma\text{-Al}_2\text{O}_3$  catalysts

Pt loading (wt%)	(a)	(b)	(c)	(d)	(e)
$0.5\text{Pt}-10\text{WO}_3/\gamma\text{-Al}_2\text{O}_3$	340	32.5	643	67.36	99.86
$1\text{Pt}-10\text{WO}_3/\gamma\text{-Al}_2\text{O}_3$	338	83.8	630	93.6	177.4
$2\text{Pt}-10\text{WO}_3/\gamma\text{-Al}_2\text{O}_3$	348	70.4	680	124.9	195.3
$3\text{Pt}-10\text{WO}_3/\gamma\text{-Al}_2\text{O}_3$	345	56.6	665	94.7	141.3

a and c –  $T_{\text{max}}$ , b and d –  $\text{H}_2$  uptake ( $\mu\text{mol g}^{-1}$ ), e – total  $\text{H}_2$  uptake ( $\mu\text{mol g}^{-1}$ ).

Table 4 Effect of  $\text{WO}_3$  loading on hydrogenation of levulinic acid to valeric acid

$\text{WO}_3$ loading (%)	Selectivity (%)					
	(a)	(b)	(c)	(d)	(e)	(f)
$2\text{Pt}-5\text{WO}_3/\gamma\text{-Al}_2\text{O}_3$	85	55	41	2	2	170
$2\text{Pt}-10\text{WO}_3/\gamma\text{-Al}_2\text{O}_3$	91	27	58	10	5	190
$2\text{Pt}-15\text{WO}_3/\gamma\text{-Al}_2\text{O}_3$	88	22	49	19	10	185
$2\text{Pt}-20\text{WO}_3/\gamma\text{-Al}_2\text{O}_3$	77	19	47	22	12	170

a – LA conversion (%), b – GVL, c – VA, d – AL, e – others, f – total acidity ( $\mu\text{mol g}^{-1}$ ). Reaction conditions: pure levulinic acid, catalyst weight 0.5 g,  $2\text{Pt}-Y\text{WO}_3/\gamma\text{-Al}_2\text{O}_3$  catalyst ( $Y = 5, 10, 15$  and  $20$  wt%), reaction temperature 270 °C, WHSV  $1.14$   $\text{h}^{-1}$  (with respect to LA), and  $\text{H}_2$  flow  $60$   $\text{mL min}^{-1}$ . GVL:  $\gamma$ -valerolactone, VA: valeric acid, AL: angelica lactone, others includes MTHF,  $\text{C}_4$ -alcohols, and  $\text{C}_5$ -alcohols.

sample shows two low-temperature peaks in the range of 70–120 °C and 180–300 °C and a high-temperature broad peak in the range of 460–640 °C. The low temperature peaks are ascribed to physisorbed and weakly bound ammonia, whereas the high temperature peak corresponds to ammonia adsorbed on the strong acidic sites, as shown in Fig. 7.

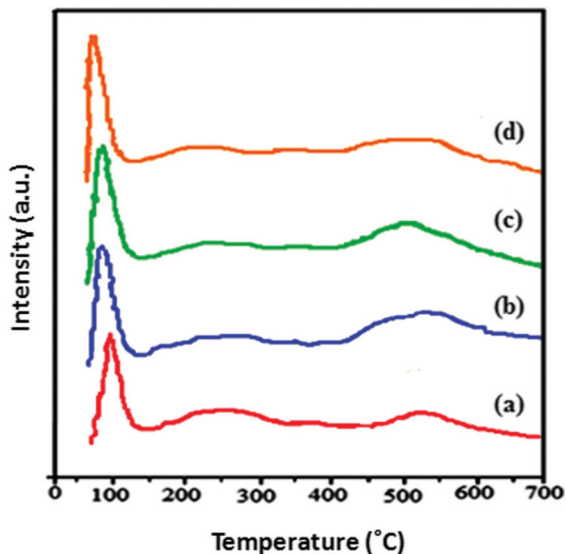


Fig. 7  $\text{NH}_3$ -TPD profiles of various 2Pt- $\text{XWO}_3/\gamma\text{-Al}_2\text{O}_3$  catalysts: (a) 2Pt-5 $\text{WO}_3/\gamma\text{-Al}_2\text{O}_3$ , (b) 2Pt-10 $\text{WO}_3/\gamma\text{-Al}_2\text{O}_3$ , (c) 2Pt-15 $\text{WO}_3/\gamma\text{-Al}_2\text{O}_3$  and (d) 2Pt-20 $\text{WO}_3/\gamma\text{-Al}_2\text{O}_3$ .

This result suggests that the introduction of  $\text{WO}_3$  led to the increased acid strength of the catalysts. The acidity of the catalyst mainly depends on the amount of the active phase of 2Pt-10 $\text{WO}_3$  present on alumina. Further, with an increase in the  $\text{WO}_3$  loading the total amount of acid sites increased steadily, reached a maximum over 2Pt-10 $\text{WO}_3/\gamma\text{-Al}_2\text{O}_3$ , and then decreased marginally.

**2.1.9 Pyridine adsorbed FTIR.** As  $\text{NH}_3$ -TPD is a useful technique to determine the acidic strength of catalysts, the pyridine adsorbed FTIR technique is another such method used to find the nature of acidic sites present in the catalyst. The pyridine adsorbed FTIR spectra of  $\text{WO}_3/\gamma\text{-Al}_2\text{O}_3$  and that of Pt- $\text{WO}_3/\gamma\text{-Al}_2\text{O}_3$  catalysts with 0.5–3 wt% loading are illustrated in Fig. 8. All bands contained in the spectra at  $1551\text{ cm}^{-1}$  are due to the presence of pyridinium ions on Brønsted acid sites,<sup>30,31</sup> at  $1455\text{ cm}^{-1}$  characteristic of Lewis sites and at  $1490\text{ cm}^{-1}$  associated with both Brønsted and Lewis sites. It can be noticed from Fig. 8 that all the catalysts contain Lewis sites, Brønsted sites and Lewis-Brønsted sites in various proportions depending upon the loading of  $\text{WO}_3$  on the support.

## 2.2 Catalytic activity

**2.2.1 Effect of  $\text{WO}_3$  loading.** The influence of  $\text{WO}_3$  loading (5 to 20 wt%) on the conversion of levulinic acid over Pt- $\text{WO}_3/\gamma\text{-Al}_2\text{O}_3$  was studied and the results obtained are shown in Table 4. As the W content increased from 5 to 10 wt%, the selectivity of GVL decreased and simultaneously the selectivity of VA and the conversion of levulinic acid increased initially and decreased later on with increasing  $\text{WO}_3$  loading beyond 10 wt%. The rise in the selectivity of VA with the inclusion of  $\text{WO}_3$  into the catalyst can be endorsed to the generation of Brønsted acid sites by  $\text{WO}_3$  species that has facilitated the ring opening of GVL to form VA.<sup>4,9</sup>

Moreover, the selectivity of VA was enhanced with the increase of  $\text{WO}_3$  loading from 5 to 10 wt%. But on further increasing the  $\text{WO}_3$  loading to 15 wt% and 20 wt%, the LA

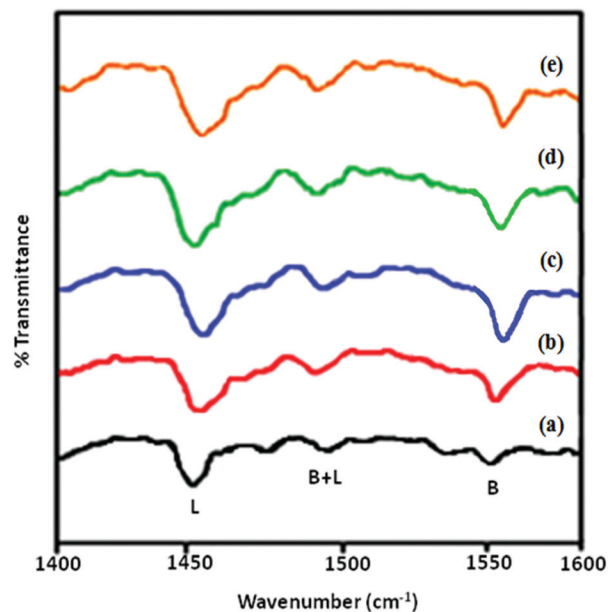


Fig. 8 Pyridine adsorbed FT-IR patterns of  $\text{WO}_3/\text{Al}_2\text{O}_3$  and various Pt- $\text{WO}_3/\text{Al}_2\text{O}_3$  catalysts. (a) 10 $\text{WO}_3/\gamma\text{-Al}_2\text{O}_3$ , (b) 0.5Pt-10 $\text{WO}_3/\gamma\text{-Al}_2\text{O}_3$ , (c) 1Pt-10 $\text{WO}_3/\gamma\text{-Al}_2\text{O}_3$ , (d) 2Pt-10 $\text{WO}_3/\gamma\text{-Al}_2\text{O}_3$  and (e) 3Pt-10 $\text{WO}_3/\gamma\text{-Al}_2\text{O}_3$ .

conversion decreased and the selectivity of VA decreased to 47%. This indicates that 10 wt%  $\text{WO}_3$  loading was found to be the optimized loading for selective conversion of LA to VA. These results are in good conformity with  $\text{NH}_3$ -TPD studies.

**2.2.2 Effect of platinum loading.** The influence of platinum loading on the hydrogenation of LA to VA over Pt- $\text{WO}_3/\gamma\text{-Al}_2\text{O}_3$  catalysts was studied. As the Pt content increases from 0.5 to 2 wt%, the LA conversion also increases from 75% to 91%. As shown in Table 5, the selectivity of VA increased with the increase of Pt loading and reached the highest (58%) at 2 wt% loading. However, a further increase in Pt loading to 3 wt% led to a slight decrease in the selectivity of VA and the results are presented in Fig. 9. This may be due to agglomeration of platinum particles on the support which blocked the acid sites and reduced the dispersion of Pt as evidenced by XRD, TEM and elemental analysis results. The catalytic activity results are in good correlation with the results obtained from acidity measurements

Table 5 Effect of Pt loading on the hydrogenation of levulinic acid to valeric acid

Pt loading (wt%)	Selectivity (%)				
	(a)	(b)	(c)	(d)	(e)
0.5Pt-10 $\text{WO}_3/\gamma\text{-Al}_2\text{O}_3$	75	58	36	2	4
1Pt-10 $\text{WO}_3/\gamma\text{-Al}_2\text{O}_3$	88	43	45	7	5
2Pt-10 $\text{WO}_3/\gamma\text{-Al}_2\text{O}_3$	91	27	58	10	5
3Pt-10 $\text{WO}_3/\gamma\text{-Al}_2\text{O}_3$	85	20	48	17	10

a - LA conversion (%), b - GVL, c - VA, d - AL, e - others. Reaction conditions: pure levulinic acid, weight of catalyst 0.5 g, XPt-10 $\text{WO}_3/\gamma\text{-Al}_2\text{O}_3$  catalyst ( $X = 0.5$  to 3.0 wt%), reaction temperature  $270\text{ }^\circ\text{C}$ , WHSV  $1.14\text{ h}^{-1}$  (with respect to LA), and  $\text{H}_2$  flow  $60\text{ mL min}^{-1}$ . GVL:  $\gamma$ -valerolactone, VA: valeric acid, AL: angelica lactone, others includes MTHF,  $\text{C}_4$ -alcohols, and  $\text{C}_5$ -alcohols.

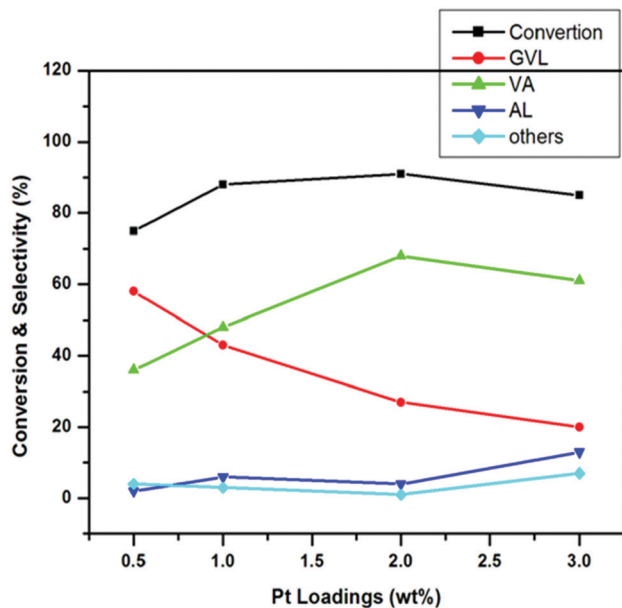


Fig. 9 Effect of platinum loading on the hydrogenation of levulinic acid over 2Pt-10WO<sub>3</sub>/γ-Al<sub>2</sub>O<sub>3</sub> catalysts.

by the NH<sub>3</sub>-TPD method. The total carbon content in used catalysts was determined by CHNS analysis and the results are presented in Table 5.

**2.2.3 Effect of weight hour space velocity (WHSV).** The influence of weight hour space velocity (WHSV) was investigated for levulinic acid hydrogenation with different flow rates of reaction feed (pure LA solution, density = 1.14 g mL<sup>-1</sup>) from 0.5 mL h<sup>-1</sup> (WHSV = 1.14 h<sup>-1</sup>) to 2.0 mL h<sup>-1</sup> (WHSV = 4.57 h<sup>-1</sup>) by keeping constant the weight of the catalyst. It is observed that the LA conversion and VA selectivity decreased from 91% to 64% and 58% to 47%, respectively, with an increase in WHSV from 1.14 h<sup>-1</sup> to 4.57 h<sup>-1</sup>. In contrast, the selectivity of other products such as GVL, AL, MTHF and others was enhanced. These results demonstrate that maximum VA selectivity was obtained at lower WHSV owing to the longer contact time. Since the available number of active sites remains unchanged the decrease in LA conversion and selectivity of VA at higher WHSV (high feed flow rate) was as expected. WHSV values were calculated using the following formula and the results are presented in Fig. 10:<sup>32</sup>

$$\text{WHSV} = \text{mass of flow (g h}^{-1}\text{)}/\text{weight of the catalyst (g)}$$

where mass of flow = feed flow rate (mL h<sup>-1</sup>) × density of feed flow (g mL<sup>-1</sup>).

**2.2.4 Effect of reaction temperature.** The influence of reaction temperature on hydrogenation of levulinic acid over the 2Pt-10WO<sub>3</sub>/γ-Al<sub>2</sub>O<sub>3</sub> catalyst in the range of 230–310 °C was investigated and the results are presented in Table 6. The levulinic acid (LA) conversion increased from 78% to 95% as the temperature increased from 230 °C to 310 °C whereas the selectivity of valeric acid (VA) reached 58% at 270 °C followed by a slight decrease at higher temperature. The optimal reaction temperature to perform hydrogenation of LA to VA selectively over a 2 wt% Pt-10WO<sub>3</sub>/Al<sub>2</sub>O<sub>3</sub> catalyst is 270 °C.

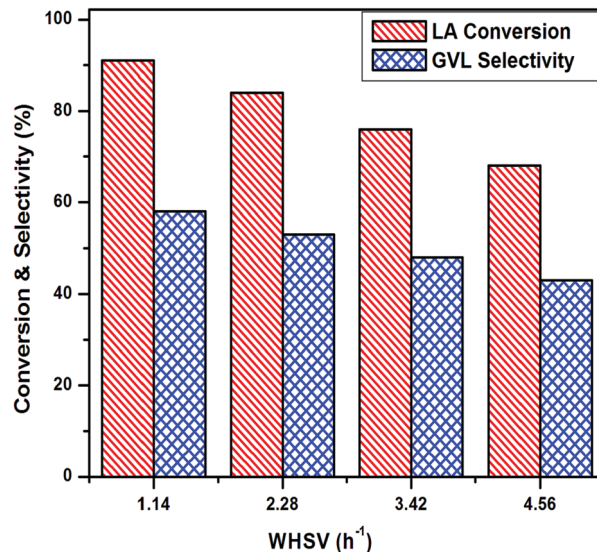


Fig. 10 Effect of WHSV on the hydrogenation of levulinic acid over 2Pt-10WO<sub>3</sub>/γ-Al<sub>2</sub>O<sub>3</sub> catalysts. Reaction conditions: pure levulinic acid, weight of catalyst 0.5 g, XPt-10WO<sub>3</sub>/γ-Al<sub>2</sub>O<sub>3</sub>, reaction temperature 270 °C, WHSV (1.14, 2.28, 3.42 and 4.56 h<sup>-1</sup> (with respect to LA)), and H<sub>2</sub> flow 60 mL min<sup>-1</sup>. GVL: γ-valerolactone, VA: valeric acid, AL: angelica lactone, others includes MTHF, C<sub>4</sub>-alcohols, and C<sub>5</sub>-alcohols.

Table 6 Effect of reaction temperature on hydrogenation of LA to VA

(a)	Selectivity (%)				
	(b)	(c)	(d)	(e)	(f)
230	78	58	36	1	5
250	87	46	49	3	2
270	91	27	58	10	5
290	93	25	49	16	10
310	95	19	45	21	15

a – temperature (°C), b – LA conversion (%), c – GVL, d – VA, e – AL, f – others. Reaction conditions: pure levulinic acid, catalyst weight 0.5 g, reaction temperature (230, 250, 270, 290 and 310 °C), WHSV 1.14 h<sup>-1</sup>, and H<sub>2</sub> flow 60 mL min<sup>-1</sup>. GVL: γ-valerolactone, VA: valeric acid, AL: angelica lactone, others includes MTHF, C<sub>4</sub>-alcohols, and C<sub>5</sub>-alcohols.

The catalytic activity mainly depends on the number of active sites located on the support. The conversion of LA to VA involves two consecutive steps: one is hydrogenation of LA to GVL and the other is ring opening of GVL followed by dehydration to VA. Hence, a catalyst used for the conversion of LA to VA should possess both acidic and metallic sites to enable dehydration and hydrogenation steps respectively. In the present study, γ-Al<sub>2</sub>O<sub>3</sub> supported platinum-tungsten catalysts demonstrated superior catalytic performance due to the presence of efficient metallic and acidic sites required for the conversion of LA to VA. The active sites on Pt facilitated the hydrogenation of LA to GVL and the acidic sites generated by incorporation of WO<sub>3</sub> species in the catalyst facilitated the ring opening of GVL followed by dehydration to VA.

**2.2.5 Time-on-stream study.** The effect of time on stream (TOS) analysis up to 60 hours of reaction time was investigated over 2Pt-10WO<sub>3</sub>/γ-Al<sub>2</sub>O<sub>3</sub> catalysts and the results are presented

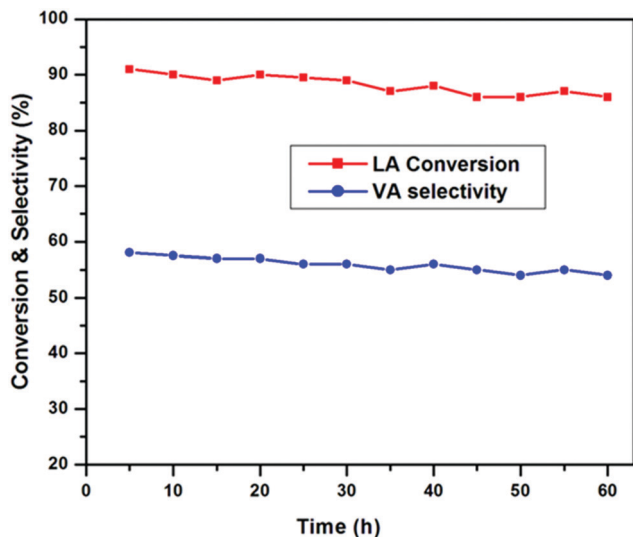


Fig. 11 Time on stream studies over 2Pt–10WO<sub>3</sub>/γ-Al<sub>2</sub>O<sub>3</sub> catalysts.

Table 7 Studies of the spent catalyst 2Pt–10WO<sub>3</sub>/Al<sub>2</sub>O<sub>3</sub>

Catalyst	(a)	(b)	(c)	(d)	(e)
Fresh	91	58	27	167	190
Spent	88	53	25	155	188

a – LA conversion (%), b – VA (%), c – GVL (%), d – BET surface area (m<sup>2</sup> g<sup>-1</sup>), e – acidity (μmol g<sup>-1</sup>).

in Fig. 11. At 5 h, the highest LA conversion and selectivity of VA were 91% and 58% respectively. However, the maximum conversion and selectivity remained stable till 25 h, and subsequently decreased with time. The time on stream results reveal that such deactivation of the catalyst could be attributed to the blocking of the active acid sites by carbon deposition as revealed by CHNS analysis presented in Table 7.

**2.2.6 Spent catalyst studies.** The spent catalyst was regenerated by activating the catalyst in air at 300 °C for 3 h followed by reduction in H<sub>2</sub> flow at 300 °C for 3 h to remove the coke deposited on the surface of the catalyst.<sup>33,34</sup> The best catalyst 2Pt–10WO<sub>3</sub>/γ-Al<sub>2</sub>O<sub>3</sub> was reused for levulinic acid hydrogenation in order to observe the catalytic performance and to study the possible reasons for deactivation. The spent catalyst was characterized by various techniques such as XRD, TEM, BET surface area, CHNS analysis and NH<sub>3</sub>-TPD. The results are shown in Table 7; the conversion of LA and selectivity of VA were slightly decreased over the used catalyst when compared to that of the fresh catalyst. By using CHNS analysis the amount of carbon deposited on the spent catalyst was deduced (Table 8) and it was noticed that the acidity and BET surface area of the spent catalyst were slightly decreased compared to the fresh catalyst

Table 8 Elemental analysis by CHNS

Catalyst	N (%)	C (%)	H (%)	S (%)
2Pt/10W–Al	—	—	0.80	0.35
Used 2Pt/10W–Al	—	5.20	1.24	0.55

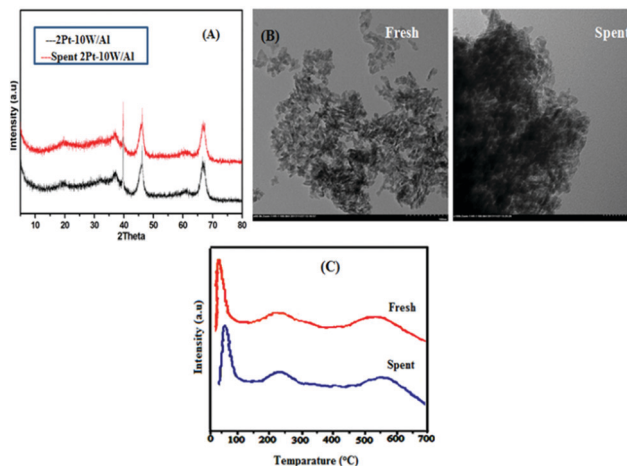


Fig. 12 (A) XRD, (B) TEM and (C) TPD images of the fresh and used 2Pt–10WO<sub>3</sub>/γ-Al<sub>2</sub>O<sub>3</sub> catalysts.

(Table 7) due to the formation of carbon on surface acid sites and blockage of mesopores. There were not many changes as observed from the TEM images and XRD patterns of the spent 2Pt–10WO<sub>3</sub>/γ-Al<sub>2</sub>O<sub>3</sub> catalyst compared to the fresh catalyst as shown in Fig. 12.

## 3. Experimental section

### 3.1 Catalyst preparation

Ammonium metatungstate hydrate ((NH<sub>4</sub>)<sub>6</sub>(H<sub>2</sub>W<sub>12</sub>O<sub>40</sub>)·H<sub>2</sub>O), chloro platinum acid hexahydrate (H<sub>2</sub>PtCl<sub>6</sub>·6H<sub>2</sub>O) and γ-Al<sub>2</sub>O<sub>3</sub> (Engelhard Corporation; BET surface area 214 m<sup>2</sup> g<sup>-1</sup>) and deionised water were used. All chemicals were used as received. A series of Pt–WO<sub>3</sub> supported γ-Al<sub>2</sub>O<sub>3</sub> catalysts were synthesized by the impregnation method. In a typical synthesis, γ-Al<sub>2</sub>O<sub>3</sub> was first impregnated with tungsten precursor ((NH<sub>4</sub>)<sub>6</sub>(H<sub>2</sub>W<sub>12</sub>O<sub>40</sub>)·H<sub>2</sub>O) solution, followed by the introduction of Pt precursor (H<sub>2</sub>PtCl<sub>6</sub>·6H<sub>2</sub>O) solution. The resulting solids were dried at 110 °C and calcined at 500 °C for 4 h in air after each impregnation step. The loading of WO<sub>3</sub> and Pt was 10 wt% and 0.5–3 wt%, respectively. The final catalysts were labeled as XPT–YWO<sub>3</sub>/γ-Al<sub>2</sub>O<sub>3</sub>, where X refers to Pt loading and Y refers to WO<sub>3</sub> loading.

### 3.2 Catalyst characterization

The X-ray diffraction (XRD) of catalysts was performed on a Rigaku miniflex X-ray diffractometer. The measurements were taken at a scan rate of 2° min<sup>-1</sup> using Ni filtered Cu Kα radiation (λ = 0.15406 nm) from 2θ = 2 to 65°, with a beam voltage of 30 kV and a beam current of 15 mA.

The surface area and pore size distribution studies of the calcined catalysts were carried out by the multipoint BET method using N<sub>2</sub> adsorption–desorption experiments at –196 °C on Autosorb 1 (Quanta Chrome Instruments).

The transmission electron microscopy (TEM) images were taken on a Hitachi HT7700 microscope operated at 100 kV. The sample grid was prepared by ultrasonically dispersing the

sample into ethanol, depositing droplets onto a carbon-coated copper grid, followed by drying in air.

The FTIR spectra of pyridine adsorbed samples were recorded on an IR (model: GC-FT-IR Nicolet 670) spectrometer by the KBr disc method to elucidate the Brønsted and Lewis acid sites. Initially the catalysts were activated in N<sub>2</sub> flow at 300 °C for 1 h to remove moisture and cooled to room temperature. This was followed by pyridine adsorption on the activated catalysts at 120 °C.

TPD experiments were carried out on an Auto Chem 2910 (Micromeritics, USA) instrument. In a typical experiment, 100 mg of dried catalyst was pretreated in high purity (99.995%) helium (50 mL min<sup>-1</sup>) at 200 °C for 1 h. After pretreatment, the sample was saturated with 10% NH<sub>3</sub>-He (50 mL min<sup>-1</sup>) at 80 °C for 1 h and subsequently flushed with He (50 mL min<sup>-1</sup>) at 80 °C for 30 min to remove physisorbed ammonia. TPD analysis was carried out from ambient temperature to 800 °C at a heating rate of 10 °C min<sup>-1</sup>.

Diffusion reflectance spectra were recorded at room temperature in the UV-visible region 200–900 nm at a split width of 1.5 nm and a scan speed of 400 nm per minute using a GBC Cintra10e UV-visible spectrometer for the catalysts. About 15 mg of the catalyst sample and dried KBr was used to make pellets by uniform mixing.

### 3.3 Catalyst testing

The vapor hydrogenation reaction was carried out in a conventional down flow fixed-bed quartz reactor (40 cm length, 9 mm i.d.) under ambient pressure. Approximately, 0.5 g of the catalyst was mixed with an equal amount of glass beads supported on the ceramic wool bed in the reactor. The catalysts were reduced at 350 °C for 2 h in a stream of H<sub>2</sub>. After cooling down to the reaction temperature (270 °C), hydrogen (60 mL min<sup>-1</sup>) and LA were introduced into the reactor. The reaction products were condensed in an ice-water trap and collected hourly for analysis on a gas chromatograph GC-2014 (Shimadzu) equipped with a DB-wax 123-7033 (Agilent) capillary column (0.32 mm i.d., 30 m long) and equipped with a flame ionization detector. The total carbon content in used catalysts was determined by using a CHNS Analyzer-ELEMENTAR Vario micro cube model. The overall carbon mass balance was found to be >98% unless otherwise stated. The conversion of levulinic acid and selectivity of products were calculated as follows:

$$\text{Conversion (\%)} = \frac{\text{moles of LA (in)} - \text{moles of LA (out)}}{\text{moles of LA (in)}} \times 100$$

$$\text{Selectivity (\%)} = \frac{\text{moles of one product}}{\text{moles of all products}} \times 100$$

## 4. Conclusions

In conclusion, tungsten oxide incorporated platinum catalysts supported on  $\gamma$ -Al<sub>2</sub>O<sub>3</sub> were successfully synthesized and applied to the hydrogenation of levulinic acid to valeric acid in flow reactors at atmospheric pressure. SEM and TEM techniques revealed the morphological aspects of the catalysts. X-ray diffraction,

temperature programmed reduction, and elemental mapping analyses showed the presence of tungsten in the synthesized catalysts. The temperature programmed desorption of ammonia and *ex situ* pyridine-FT-IR studies demonstrated the acidity of the catalysts. Under optimized reaction conditions, the 2Pt-10WO<sub>3</sub>/ $\gamma$ -Al<sub>2</sub>O<sub>3</sub> catalyst exhibited the highest selectivity (58%) to valeric acid with 91% conversion of LA. The greater catalytic performance of the catalyst is attributed to the enhanced acidity due to the incorporation of tungsten oxide, high surface area, greater dispersion of Pt and the synergistic interaction between active species and the support. The 2Pt-10WO<sub>3</sub>/ $\gamma$ -Al<sub>2</sub>O<sub>3</sub> catalyst showed quite stable catalytic activity during the 60 h time on stream. The slight decrease in the selectivity to VA is due to the deposition of carbonaceous species over the catalyst surface.

## Conflicts of interest

There are no conflicts to declare.

## Acknowledgements

PB thanks University Grants Commission (UGC), New Delhi, for the award of a Senior Research Fellowship and KVR thanks CSIR, New Dehi, for financial support under the Emeritus Scientist scheme.

## References

- 1 B. Putrakumar, N. Nagaraju, V. Pavan Kumar and K. V. R. Chary, *Catal. Today*, 2014, **7**, 014.
- 2 X. Shaodan, Y. Deqing, Y. Tao and T. Panpan, *RSC Adv.*, 2017, **7**, 1026.
- 3 N. P. Jindrayani, K. Alfin, E. S. Felycia, L. Shi-Yow, J. Yi-Hsu and I. Suryadi, *RSC Adv.*, 2015, **5**, 41285.
- 4 V. V. Kumar, G. Naresh, S. Deepa, P. G. Bhavani, M. Nagaraju, M. Sudhakar, K. V. R. Chary, J. Tardio, S. K. Bhargava and A. Venugopal, *Appl. Catal., A*, 2016, **10**, 032.
- 5 B. Kamm, P. R. Gruber and M. Kamm, *Chem. Rev.*, 2006, **106**, 4044.
- 6 J. J. Bozell, *Science*, 2010, **329**, 522–523.
- 7 K. Kon, W. Onodera and K. I. Shimizu, *Catal. Sci. Technol.*, 2014, **4**, 3227–3234.
- 8 Y. Qiu, L. Xin, D. J. Chadderton, J. Qi, C. Liang and W. Li, *Green Chem.*, 2014, **16**, 1305–1315.
- 9 D. J. Hayes, S. Fitzpatrick, M. H. B. Hayes and J. R. H. Ross, in *Biorefineries: Industrial Processes and Products*, ed. B. Kamm, P. R. Gruber, M. Kamm, Wiley-VCH, Weinheim, 2006, vol. 2, pp.139–164.
- 10 I. T. Horvath, H. Mehdi, V. Fabos, L. Boda and L. T. Mika, *Green Chem.*, 2008, **10**, 238–242.
- 11 S. V. D. Vyver, J. Thomas, J. Geboers, S. Keyzer, M. Smet, W. Dehaen, P. A. Jacobsa and B. F. Sels, *Energy Environ. Sci.*, 2011, **4**, 3601.
- 12 J. Xin, D. Yan, O. Ayodele, Z. Zhang, X. Lu and S. Zhang, *Green Chem.*, 2015, **17**, 1065–1070.

- 13 X. L. Du, Q. Y. Bi, Y. M. Liu, Y. Cao, H. Y. He and K. N. Fan, *Green Chem.*, 2012, **14**, 935–939.
- 14 J. Q. Bond, D. M. Alonso, R. M. West and J. A. Dumesic, *Langmuir*, 2010, **26**, 16291–16298.
- 15 C. E. Chan-Thaw, M. Marelli, R. Psaro, N. Ravasio and F. Zaccheria, *RSC Adv.*, 2013, **3**, 1302–1306.
- 16 W. Luo, P. C. A. Bruijninx and B. M. Weckhuysen, *J. Catal.*, 2014, **320**, 33–41.
- 17 N. P. Jindrayani, K. Alfin, E. S. Felycia, L. Shi-Yow, J. Yi-Hsu and I. Suryadi, *RSC Adv.*, 2015, **5**, 41285.
- 18 J. P. Lange, R. Price, P. M. Ayoub, J. Louis, L. Petrus, L. Clarke and K. H. Gosselin, *Angew. Chem., Int. Ed.*, 2010, **49**, 4479–4483.
- 19 K. Kon, W. Onodera and K. I. Shimizu, *Catal. Sci. Technol.*, 2014, **4**, 3227–3234.
- 20 T. Pan, J. Deng, Q. Xu, Y. Xu, Q. X. Guo and Y. Fu, *Green Chem.*, 2013, **15**, 2967–2974.
- 21 P. Bhanuchander, S. S. Priya, V. P. Kumar, S. K. Hussain, N. P. Rajan, S. K. Bhargava and K. V. R. Chary, *Catal. Lett.*, 2017, **147**, 845–855.
- 22 J. S. Valente, M. S. Cantu, J. G. H. Cortez, R. Montiel, X. Bokhimi and E. L. Salinas, *J. Phys. Chem.*, 2007, **111**, 642–651.
- 23 P. S. Dutta and A. Khanna, *ECS J. Solid State Sci. Technol.*, 2013, **2**, R3153–R3167.
- 24 E. P. Parry, *J. Catal.*, 1963, **2**, 371–379.
- 25 J. A. Horsley, I. E. Wachs, J. M. Brown, G. H. Via and F. D. Hardcastle, *J. Phys. Chem.*, 1987, **91**, 4014–4020.
- 26 S. S. Priya, V. P. Kumar, M. L. Kantam, S. K. Bhargava, A. Srikanth and K. V. R. Chary, *Ind. Eng. Chem. Res.*, 2015, **54**(37), 9104–9115.
- 27 J. A. Horsley, I. E. Wachs, J. M. Brown, G. H. Via and F. D. Hardcastle, *J. Phys. Chem.*, 1987, **91**, 4014–4020.
- 28 A. D. Lucas, J. L. Valverde, P. Canizares and L. Rodriguez, *Appl. Catal., A*, 1998, **172**, 165–176.
- 29 X. L. Yang, W. L. Dai, R. Gao and K. Fan, *J. Catal.*, 2007, **249**, 278–288.
- 30 S. S. Priya, V. P. Kumar, M. L. Kantam, S. K. Bhargava and K. V. R. Chary, *RSC Adv.*, 2014, **4**, 51893.
- 31 S. S. Priya, P. Bhanuchander, V. P. Kumar, D. Deepa, P. R. Selvakannan, M. L. Kantam, S. K. Bhargava and K. V. R. Chary, *ACS Sustainable Chem. Eng.*, 2016, **4**, 1212–1222.
- 32 S. S. Priya, P. Bhanuchander, V. P. Kumar, S. K. Bhargava and K. V. R. Chary, *Ind. Eng. Chem. Res.*, 2016, **55**, 4461–4472.
- 33 S. S. Priya, V. P. Kumar, M. L. Kantam, S. K. Bhargava and K. V. R. Chary, *RSC Adv.*, 2014, **4**, 51893–51903.
- 34 S. S. Priya, V. P. Kumar, M. L. Kantam, S. K. Bhargava and K. V. R. Chary, *Catal. Lett.*, 2014, **144**, 2129–2143.